Journal of Sound and Vibration (2001) , 000–000

Merging sensor data from multiple measurement setups for nonstationary subspace-based modal analysis

Laurent Mevel, Michèle Basseville, Albert Benveniste, Maurice Goursat

L.M., M.B. and A.B. are with Irisa, *Campus de Beaulieu, 35042 Rennes Cedex, F.*
L.M. and A.B. are also with Inria, *and M.B. is also with* Cnrs.
M.G. is with Inria, *BP 105, Rocquencourt, 78153 Le Chesnay Cedex, F.*

Corresponding author: Michèle Basseville,
Irisa, Campus de Beaulieu, 35042 Rennes Cedex, France.
basseville@irisa.fr, Tel +33 2 99 84 72 36, Fax +33 2 99 84 71 71.

Abstract

Processing sensor data, from multiple non-simultaneously recorded measurement setups, for structural analysis is often achieved by merging identification results obtained from records corresponding to different sensor pools. Since pole matching and eigenvector gluing might not be consistent in some cases, the question arises to merge the data first and then process them globally. Subspace identification algorithms have proven efficient for performing output-only modal analysis of mechanical systems subject to uncontrolled, unmeasured, and nonstationary excitation. The purpose of this paper is to investigate how subspace-based output-only modal analysis algorithms can be adapted to handle the polyreference setup. Numerical results, obtained on both a laboratory and a real application examples, are reported, which show the relevance and usefulness of the proposed algorithm.

© 2001 Academic Press

1. INTRODUCTION

A major issue for in-operation structural vibration analysis, based on measurements from accelerometers or strain gauges, is to identify modes and modal shapes of mechanical systems subject to an uncontrolled, *unmeasured* and *nonstationary* excitation [1, 2]. Typical examples are offshore structures subject to swell, buildings subject to wind or earthquake, bridges subject to traffic, dams,

© 2001 Academic Press

wings subject to flutter in flight, and turbines subject to steam turbulence, friction in bearings, and imperfect balancing. Modeling modes and modal shapes through state space representations [3, 4, 5] shows that structural analysis is an important instance of identification of the eigenstructure of a linear multi-variable system [6, 7, 8]. For linear system identification, subspace-based methods [9, 10, 11] have proven efficient.

In-operation structural analysis calls for the use of *output-only* identification methods [12, 13]. The nonstationarity of the unknown excitation also calls for processing long samples of multi-sensor output measurements, and for using *covariance-driven* subspace-based identification methods [14, 15].

A common practice in structural analysis is to collect data from varying sensor locations, using both fixed and moving sensors, in order to mimic the availability of a (much) larger set of sensors. Several successive data sets are recorded, with sensors at different locations on the structure. Some of the sensors, called the *reference* sensors, are kept fixed, while the others are moved. This setup is referred to as *polyreference* setup in this paper. Typically, it is based on about ten sensors, and can mimic a situation in which hundreds of sensors are available.

Processing polyreference data for structural analysis is often achieved by performing eigenstructure identification for each record separately, and then merging the results obtained for records corresponding to different sensor pools. However, pole matching may be not easy in practice, and thus the result of eigenvector gluing may not be consistent [16, 17]. Therefore the question arises to perform eigenstructure identification by merging the data of the successive records, and processing them globally, instead of merging the

identification results.

The purpose of this paper is to investigate how subspace-based output-only modal analysis algorithms can be adapted to handle a polyreference setup, in the presence of an unmeasured and nonstationary excitation.

In section 2, we introduce the models and briefly review output-only covariance-driven subspace-based modal analysis methods. The mathematical modeling of the polyreference setup is stated in section 3. A first merge of data is proposed for the case of a stationary excitation. This merge is shown to fail in the case of a nonstationary excitation. For the latter case, a covariance normalization prior to merge is introduced, and a simple implementation is given. Numerous experimental results obtained, on both a laboratory and a real application examples, are reported in section 4. Finally, some conclusions are drawn in section 5.

2. OUTPUT-ONLY SUBSPACE-BASED MODAL ANALYSIS

In this section, we briefly review structural vibration analysis and subspace-based identification algorithms. First, we introduce the modeling issues, and then we recall output-only covariance-driven subspace identification.

2.1. MODELING

The use of state-space representations for modal analysis is well known [3, 4, 12]. In order to introduce the notations we use, we briefly recall the main equations and parameters. We assume that the behavior of the mechanical system can be described by a stationary linear dynamical system, and that, in the frequency range of interest, the input forces can be modeled as a nonstationary white noise. This results in the following matrix differential

equation :

$$\begin{cases} M\ddot{\mathcal{Z}}(t) + C\dot{\mathcal{Z}}(t) + K\mathcal{Z}(t) = \nu(t) \\ Y(t) = L\mathcal{Z}(t) \end{cases} \tag{1}$$

where t denotes continuous time, M, C, K are the mass, damping and stiffness matrices respectively, (high dimensional) vector $\mathcal{Z}$ collects the displacements or accelerations of the degrees of freedom of the structure; the external (non measured) force ν is modeled as a nonstationary white noise with time-varying covariance matrix $Q_\nu(t)$, measurements are collected in the (often, low dimensional) vector Y, and matrix L indicates which components of the state vector are actually measured (where the sensors are located). The modes or eigenfrequencies denoted generically by μ, and the mode shapes or eigenvectors denoted generically by ψ_μ, are solutions of:

$$\det(M\mu^2 + C\mu + K) = 0 \ , \quad (M\mu^2 + C\mu + K)\ \Psi_\mu = 0 \ , \quad \psi_\mu = L\ \Psi_\mu \tag{2}$$

Sampling the model in (1) at rate $1/\tau$ yields the discrete time model in state space form:

$$\begin{cases} X_{k+1} = F\ X_k + V_{k+1} \\ Y_k = H\ X_k \end{cases} \tag{3}$$

where the state and the output are:

$$X_k = \begin{bmatrix} \mathcal{Z}(k\tau) \\ \dot{\mathcal{Z}}(k\tau) \end{bmatrix} \ , \ Y_k = Y(k\tau), \tag{4}$$

the state transition and observation matrices are:

$$F = e^{\mathcal{L}\tau} \ , \ \mathcal{L} = \begin{bmatrix} 0 & I \\ -M^{-1}K & -M^{-1}C \end{bmatrix} \ , \ H = \begin{bmatrix} L\ 0 \end{bmatrix},$$

and where state noise V_{k+1} is *unmeasured*, Gaussian, zero-mean, white, with covariance matrix:

$$Q_{k+1} \stackrel{\text{def}}{=} \mathbf{E}\left(V_{k+1}\, V_{k+1}^T\right) = \int_{k\tau}^{(k+1)\tau} e^{\mathcal{L}s}\, \widetilde{Q}(s)\, e^{\mathcal{L}^T s} ds$$

where $\mathbf{E}(.)$ denotes the expectation operator and:

$$\widetilde{Q}(s) = \begin{bmatrix} 0 & 0 \\ 0 & M^{-1} Q_\nu(s) M^{-T} \end{bmatrix}$$

The whiteness assumption on the state noise and the absence of measurement noise in (3) are discussed in section 3.4.3. We stress that sinusoidal or colored noise excitation can be encompassed as well [5]. State X and observed output Y have dimensions $2m$ and r respectively, with r (often much) smaller than $2m$ in practice. These issues are further discussed in section 4.

The modal parameters defined in (2) are equivalently found in the eigenstructure (λ, Φ_λ) of the state transition matrix F:

$$e^{\tau\mu} = \lambda, \quad \psi_\mu = \varphi_\lambda \stackrel{\text{def}}{=} H\ \Phi_\lambda$$

Eigenvectors are real if proportional damping is assumed, that is $C = \alpha M + \beta K$. Because of the structure of the state in (4), the λ's and φ_λ's are pairwise complex conjugate. We assume that the system has no multiple eigenvalues. In addition, 0 is *not* an eigenvalue of state transition matrix F. The collection of pairs $(\lambda, \varphi_\lambda)$ form a canonical parameterization[1] of the pole part of the system in (3), referred to as the system eigenstructure.

2.2. OUTPUT-ONLY COVARIANCE-DRIVEN SUBSPACE IDENTIFICATION

Processing output covariance matrices is of interest for very large data sets, especially under nonstationary excitation. The difference between the

[1] A parameterization invariant w.r.t. changes in the state basis.

covariance-driven form of subspace algorithms which we describe and the usual data-driven form [10] is minor, at least for eigenstructure identification [12].

Covariance-driven subspace identification of the eigenstructure $(\lambda, \varphi_\lambda)$'s is based on the following steps. Let $R_i \stackrel{\text{def}}{=} \mathbf{E}\, Y_k\, Y_{k-i}^T$ and

$$\mathcal{H}_{p+1,q} \stackrel{\text{def}}{=} \begin{pmatrix} R_0 & R_1 & \vdots & R_{q-1} \\ R_1 & R_2 & \vdots & R_q \\ \vdots & \vdots & \vdots & \vdots \\ R_p & R_{p+1} & \vdots & R_{p+q-1} \end{pmatrix} \stackrel{\text{def}}{=} \text{Hank}\,(R_i) \tag{5}$$

be the theoretical output-covariance and Hankel matrices, respectively. Introducing the cross-covariance between the state and the observed outputs:

$$G \stackrel{\text{def}}{=} \mathbf{E}\, X_k\, Y_k^T,$$

direct computations of the R_i's from the model equations lead to

$$R_i = H\, F^i\, G \tag{6}$$

and to the well known [18] factorization

$$\mathcal{H}_{p+1,q} = \mathcal{O}_{p+1}(H,F)\, \mathcal{C}_q(F,G) \tag{7}$$

where

$$\mathcal{O}_p(H,F) \stackrel{\text{def}}{=} \begin{pmatrix} H \\ HF \\ \vdots \\ HF^{p-1} \end{pmatrix} \quad \text{and} \quad \mathcal{C}_q(F,G) \stackrel{\text{def}}{=} (G\ FG\ \cdots\ F^{q-1}G)$$

are the observability and controllability matrices, respectively.

The observation matrix H is then found in the first block-row of the observability matrix $\mathcal{O}$. The state-transition matrix F is obtained from the shift invariance property of $\mathcal{O}$, namely:

$$\mathcal{O}_p^{\uparrow}(H,F) = \mathcal{O}_p(H,F)\ F, \qquad \text{where} \quad \mathcal{O}_p^{\uparrow}(H,F) \stackrel{\text{def}}{=} \begin{pmatrix} HF \\ HF^2 \\ \vdots \\ HF^p \end{pmatrix}$$

Of course, for recovering F, we need to assume that $\text{rank}(\mathcal{O}_p) = \dim F$, and thus that the number of block-rows in $\mathcal{H}_{p+1,q}$ is large enough. The eigenstructure (λ, Φ_λ) results from:

$$\det(F - \lambda\ I) = 0\ , \quad F\ \Phi_\lambda = \lambda\ \Phi_\lambda$$

The actual implementation of this subspace algorithm, known under the name of balanced realization (BR) [19, 20] has the empirical covariances

$$\widehat{R}_i = \frac{1}{N}\ \sum_{k=1}^{N} Y_k\ Y_{k-i}^T \tag{8}$$

substituted for R_i in $\mathcal{H}_{p+1,q}$, yielding the empirical Hankel matrix $\widehat{\mathcal{H}}_{p+1,q} \stackrel{\text{def}}{=} \text{Hank}\left(\widehat{R}_i\right)$. How to select the number of lags $(p+q)$ and thus the size of $\widehat{\mathcal{H}}_{p+1,q}$ is discussed in section 3.4.3. The SVD of $\widehat{\mathcal{H}}_{p+1,q}$ and its truncation at the desired model order yield, in the left factor, an estimate $\widehat{\mathcal{O}}$ for the observability matrix $\mathcal{O}$:

$$\begin{aligned} \widehat{\mathcal{H}} &= U\ \Delta\ V^T \\ &= U\ \begin{pmatrix} \Delta_1 & 0 \\ 0 & \Delta_0 \end{pmatrix}\ V^T \\ \widehat{\mathcal{O}} &= U\ \Delta_1^{1/2}, \qquad \widehat{\mathcal{C}} = \Delta_1^{1/2}\ V^T \end{aligned}$$

From $\widehat{\mathcal{O}}$, estimates $(\widehat{H}, \widehat{F})$ and $(\widehat{\lambda}, \widehat{\Phi}_\lambda)$ are recovered as sketched above.

The CVA algorithm basically applies the same procedure to a Hankel matrix pre- and post-multiplied by the covariance matrix of future and past data, respectively [21, 22].

The key feature in this algorithm is the factorization in (6), resulting in the factorization in (7), where the left factor $\mathcal{O}$ only depends on the pair (H, F), and thus on the eigenstructure of the system in (3), whereas the excitation V_k only affects the right factor $\mathcal{C}$ through the cross-covariance matrix G. This feature is now elaborated on for handling polyreference setups.

3. POLYREFERENCE SUBSPACE-BASED MODAL ANALYSIS

Instead of a single record for the output (Y_k) of system (3), we now have J records

$$\underbrace{\begin{pmatrix} Y_k^{(0,1)} \\ Y_k^{(1)} \end{pmatrix}}_{\text{Record 1}} \underbrace{\begin{pmatrix} Y_k^{(0,2)} \\ Y_k^{(2)} \end{pmatrix}}_{\text{Record 2}} \cdots \underbrace{\begin{pmatrix} Y_k^{(0,J)} \\ Y_k^{(J)} \end{pmatrix}}_{\text{Record } J} \tag{9}$$

collected successively. Each record j contains data $Y_k^{(0,j)}$ from a fixed *reference* sensor pool, and data $Y_k^{(j)}$ from a *moving* sensor pool. The number of sensors may be different in the fixed and the moving pools, and thus in each record j, the dimensions r_0 of $Y_k^{(0,j)}$ and r_j of $Y_k^{(j)}$ may be different. This is referred to as *polyreference setup* in the sequel.

The rest of the section is organized as follows. First, we state the mathematical modeling of the polyreference setup. Then, a first merge of data is proposed for the stationary excitation case, and is shown to fail in the non-stationary one. For the latter case, a covariance normalization prior to merge is introduced, and its implementation is given.

To each record j ($1 \leq j \leq J$) corresponds a state-space realization in the form

$$\begin{cases} X_{k+1}^{(j)} &= F\ X_k^{(j)} + V_{k+1}^{(j)} \\ Y_k^{(0,j)} &= H_0\ X_k^{(j)} \qquad \text{(reference pool)} \\ Y_k^{(j)} &= H_j\ X_k^{(j)} \qquad \text{(sensor pool n}^o j) \end{cases} \tag{10}$$

with a single state transition matrix F - since the same system is being observed, a fixed observation matrix H_0 for the fixed sensor pool, and a specific observation matrix H_j corresponding to location j of the moving sensor pool.

The problem is to find how to adapt the output-only covariance-driven subspace algorithm of section 2 in order to identify the eigenstructure of F in (10), on the basis of the measurements (9) which we should merge somehow for this purpose. At this point, two facts should be stressed. First, the cornerstone in section 2 is factorization (6) which, of course, holds for each of the J records with a *different* left factor H and a *different* right factor G. In particular, even though we do have access to empirical estimates of the covariances $\mathbf{E}\ Y_k^{(j)}\ {Y_{k-i}^{(j)}}^T$ of the moving sensor pool, they are of poor help because their factorizations (6) show up a record-dependent state-output correlation G since the sensors location change. Second, we have no access to cross-record covariances $\mathbf{E}\ Y_k^{(j')}\ {Y_{k-i}^{(j)}}^T$ with $j \neq j'$, since sensor pools j and j' do not record data simultaneously. Thus, we cannot stack all the data sets in a unique vector, otherwise we would have to handle incomplete covariance matrices.

A consequence of those two facts, in the perspective of building a Hankel matrix enjoying a factorization property, is to concentrate on the covariances

involving the *reference sensors*. From now on, we thus focus on the two following families of covariances

$$R_i^{0,j} \stackrel{\text{def}}{=} \mathbf{E}\, Y_k^{(0,j)}\, Y_{k-i}^{(0,j)^T}, \quad R_i^j \stackrel{\text{def}}{=} \mathbf{E}\, Y_k^{(j)}\, Y_{k-i}^{(0,j)^T} \tag{11}$$

of which we can compute empirical estimates, for lags $i \geq 0$. For describing the proposed solution to polyreference subspace identification, we distinguish between stationary and nonstationary input excitation cases. A first merge of the data is now proposed for the stationary input excitation case. For investigating the nonstationary case, we start with the simplifying assumption of stationary excitation within the records, and record-dependent covariance matrix. This data merging is shown to fail in that nonstationary case. In section 3.4, an alternative merge of the data is introduced, based on a covariance normalization prior to merge is proposed for the simplified case of record-dependent excitation, and its implementation is given. The truly nonstationary case, where the excitation is time-varying within each record, is a more realistic, yet much more difficult, situation to cope with. The interested reader is referred to [23] for technical details of theorems proving that the proposed method still works in that case.

3.2. DATA MERGING IN THE STATIONARY CASE

In the stationary case, the excitation covariance matrix does not depend on record j: $\mathbf{E}\, V_k^{(j)} V_{k'}^{(j)^T} = Q\ \delta(k-k')$, and the cross-covariance between the state and the fixed sensors output

$$G \stackrel{\text{def}}{=} \mathbf{E}\, X_k^{(j)}\, Y_k^{(0,j)^T}$$

does *not* depend on j either. Therefore, for all the records $j = 1, \ldots, J$ and lags $i \geq 0$, the covariances in (11) factorize, with a constant *right* factor, as

$$\begin{aligned} R_i^{0,j} &= H_0 \; F^i \; G \quad \stackrel{\text{def}}{=} \quad R_i^0 \\ R_i^j &= H_j \; F^i \; G \end{aligned} \tag{12}$$

Consequently, for each lag $i \geq 0$, we can stack the R_i^j's into a block-column vector

$$R_i^\pi \stackrel{\text{def}}{=} \begin{pmatrix} R_i^0 \\ R_i^1 \\ \vdots \\ R_i^J \end{pmatrix} \tag{13}$$

which factorizes as

$$R_i^\pi = H \; F^i \; G \tag{14}$$

where H is the block-column of observation matrices

$$H \stackrel{\text{def}}{=} \begin{pmatrix} H_0 \\ H_1 \\ \vdots \\ H_J \end{pmatrix} \tag{15}$$

Therefore, the Hankel matrix filled with those column-stacked covariances [2] factorizes as

$$\mathcal{H}^\pi \stackrel{\text{def}}{=} \text{Hank}\,(R_i^\pi) \;=\; \mathcal{O}(H, F)\, \mathcal{C}(F, G) \tag{16}$$

and the algorithm described in section 2 for the standard case can be applied to $\mathcal{H}^\pi$. In other words, when the input excitation is stationary, we can proceed

[2] This Hankel matrix has $(J + 1)$ times as many rows as columns.

as if we had the full set of sensor data available altogether, instead of sensor pools with varying locations. In this case, direct application of the subspace algorithm to the column-stacked covariances (13) is a simple solution to the polyreference output-only eigenstructure identification problem.

3.3. WHY THIS MERGE FAILS UNDER NONSTATIONARY EXCITATION

If we assume that the input excitation covariance matrix depends on the record index j:

$$\mathbf{E}\ V_k^{(j)}\ V_{k'}^{(j)^T} = Q_j\ \delta(k-k') \tag{17}$$

the cross-covariance matrix

$$G_j \stackrel{\text{def}}{=} \mathbf{E}_j\ X_k^{(j)}\ Y_k^{(0,j)^T}$$

also *depends on* j. Hence, for $j = 1, \ldots, J$ and $i \geq 0$, factorizations (12) now write with a record-dependent G

$$R_i^{0,j} = H_0\ F^i\ G_j \tag{18}$$

$$R_i^j = H_j\ F^i\ G_j \tag{19}$$

and vector R_i^π of stacked covariances defined in (13) no longer factorizes as in (14). As a consequence, brute force application of subspace algorithm by stacking the R_i^j's is not an appropriate solution to the eigenstructure identification problem in the case of record-dependent input excitation noise. To circumvent this difficulty, the idea is to *normalize* the covariance matrices (18)-(19) to make them looking as if they were obtained with the same excitation.

For finding the appropriate normalization of the covariances, we perform different covariance stacking operations for the data from the reference and moving sensors, respectively. In what follows, we use the generic notations introduced in section 2.

3.4.1. *Reference sensors*

Thanks to (18), all the Hankel matrices built on the data delivered by the reference sensors of the J records factorize with the same *left* factor as

$$\mathcal{H}_{0,j} \stackrel{\text{def}}{=} \text{Hank}\left(R_i^{(0,j)}\right) = \mathcal{O}(H_0, F)\, \mathcal{C}(F, G_j) \tag{20}$$

We can thus proceed as follows. Let $R_i^0 \stackrel{\text{def}}{=} \left(R_i^{0,1}\ R_i^{0,2}\ \ldots\ R_i^{0,J}\right)$ be the block-row vector of the entire set of reference data covariances. It factorizes as

$$R_i^0 = H_0\, F^i\, G, \quad \text{where } G \stackrel{\text{def}}{=} (\, G_1\, G_2\, \ldots\, G_J) \tag{21}$$

Thus the Hankel matrix filled with those row-stacked covariances[3] also factorizes as

$$\mathcal{H}_0 \stackrel{\text{def}}{=} \text{Hank}\left(R_i^0\right) = \mathcal{O}(H_0, F)\, \mathcal{C}(F, G) \tag{22}$$

Note that matrix $\mathcal{H}_0$ can be obtained by interleaving the block-columns of the J Hankel matrices $\mathcal{H}_{0,j}$ in (20). Assume that pair (H_0, F) is observable. Then, partitioning the right factor $\mathcal{C}$ of (22) in the same manner as G in (21), we recover the right factors $\mathcal{C}(F, G_j)$ of (20) for all $j = 1, \ldots, J$. Note that processing the reference data $Y_k^{(0,j)}$ *altogether*, on the basis of the *single* Hankel matrix factorization (22), is mandatory for making sure that we deal with the *same* state bases in (10).

[3] This Hankel matrix has J times as many columns as rows.

3.4.2. *Moving sensors*

Thanks to (19), the Hankel matrix built on the covariances of the data $Y_k^{(j)}$ from the moving sensor pool in record j enjoys a record-dependent factorization

$$\mathcal{H}_j \stackrel{\text{def}}{=} \text{Hank}\left(R_i^j\right) = \mathcal{O}(H_j, F)\, \mathcal{C}(F, G_j) \tag{23}$$

Assume that, for all j, the pair (F, G_j) is controllable[4] and that, up to a permutation on the record indexes, $\mathcal{C}(F, G_1)$ is the best conditioned controllability matrix among the $\mathcal{C}(F, G_j)$'s. For all j, $j = 1, \ldots, J$, we define the normalized matrices

$$\overline{\mathcal{H}}_j \stackrel{\text{def}}{=} \mathcal{H}_j \left(\mathcal{C}^T(F, G_j) \left(\mathcal{C}(F, G_j)\mathcal{C}^T(F, G_j)\right)^{-1} \mathcal{C}(F, G_1)\right) \tag{24}$$

We note that $\overline{\mathcal{H}}_j$ coincides with the Hankel matrix Hank $\left(\overline{R}_i^j\right)$ built on covariances $\overline{R}_i^j$ which factorize as

$$\overline{R}_i^j = H_j\ F^i\ G_1 \tag{25}$$

Therefore, we can now proceed as in the case of constant excitation covariance matrix. For each lag $i \geq 0$, we define the block-column stacked covariances

$$\overline{R}_i \stackrel{\text{def}}{=} \begin{pmatrix} \overline{R}_i^0 \\ \overline{R}_i^1 \\ \vdots \\ \overline{R}_i^J \end{pmatrix}, \quad \text{where } \overline{R}_i^0 \stackrel{\text{def}}{=} R_i^{0,1} = H_0\ F^i\ G_1 \tag{26}$$

[4] This is a reasonable assumption, it just tells that, while the excitation may change, we need it to excite all the modes of the system, for each data set.

Thanks to (25), those stacked covariances $\overline{R}_i$ behave as R_i^π defined in (13): they factorize as $\overline{R}_i = HF^iG_1$, with H defined in (15). Therefore, the Hankel matrix filled with those column-stacked covariances [5] factorizes as

$$\overline{\mathcal{H}} \stackrel{\text{def}}{=} \text{Hank}\left(\overline{R}_i\right) = \mathcal{O}(H,F)\,\mathcal{C}(F,G_1) \tag{27}$$

Note that matrix $\overline{\mathcal{H}}$ can be obtained by interleaving the block-rows of $\overline{\mathcal{H}}_0 \stackrel{\text{def}}{=} \text{Hank}\left(\overline{R}_i^0\right) = \mathcal{H}_{0,1}$ and of the J matrices $\overline{\mathcal{H}}_j$ defined in (24). Thanks to (27), the algorithm given in section 2 can be applied to $\overline{\mathcal{H}}$.

3.4.3. *Algorithm*

For implementing the above reasoning, we propose the following algorithm, where J is the number of records and $\widehat{M}$ denotes an empirical estimate of matrix M.

- Build the J Hankel matrices $\widehat{\mathcal{H}}_{0,j} = \text{Hank}\left(\widehat{R}_i^{(0,j)}\right)$ from the reference sensor data.
- Build $\widehat{\mathcal{H}}_0$ by interleaving the block-columns of the J matrices $\widehat{\mathcal{H}}_{0,j}$'s ($j = 1,\ldots,J$).
- SVD-decompose $\widehat{\mathcal{H}}_0$. Keep only the right factor $\mathcal{C}(F,G)$ in (22), and call it just $\mathcal{C}$.
- Partition $\mathcal{C}$ into $\mathcal{C} \stackrel{\text{def}}{=} (\mathcal{C}_1\ \mathcal{C}_2\ \ldots\ \mathcal{C}_J)$ as G in (21). Assume $\mathcal{C}_1$ is the best conditioned of the $\mathcal{C}_j$'s.
- Compute the normalizing factors $\left(\mathcal{C}_j^T\ (\mathcal{C}_j\,\mathcal{C}_j^T)^{-1}\,\mathcal{C}_1\right)$.
- Build the J Hankel matrices $\widehat{\mathcal{H}}_j = \text{Hank}\left(\widehat{R}_i^j\right)$ from the moving sensor data.

[5] This Hankel matrix has $(J+1)$ times as many rows as columns.

- Compute the J normalized matrices $\overline{\widehat{\mathcal{H}}}_j \stackrel{\text{def}}{=} \widehat{\mathcal{H}}_j \left(\mathcal{C}_j^T \, (\mathcal{C}_j \, \mathcal{C}_j^T \,)^{-1} \, \mathcal{C}_1 \right)$. Define $\overline{\widehat{\mathcal{H}}}_0 \stackrel{\text{def}}{=} \widehat{\mathcal{H}}_{0,1}$.
- Build $\widehat{\overline{\mathcal{H}}}$ by interleaving the block-rows of the $(J+1)$ matrices $\overline{\widehat{\mathcal{H}}}_j$'s ($j = 0, \ldots, J$).
- Apply the algorithm of section 2 to $\widehat{\overline{\mathcal{H}}}$.

The following comments are in order. First, the computational complexity of this algorithm does *not* depend on the number J of records, since the smallest dimension of the two Hankel matrices $\widehat{\mathcal{H}}_0$ and $\widehat{\overline{\mathcal{H}}}$ to be decomposed depends only on the number of reference sensors. Second, the interleaving of the block-rows of the $\overline{\widehat{\mathcal{H}}}_j$'s can be done even when the number of sensors in the moving pools is *not* constant: the measurement vectors $Y_k^{(j)}$ and $Y_k^{(j')}$ may have different dimensions. Third, we do not need to compute explicitly the G_j matrices, since only the right factors $\mathcal{C}(F, G_j)$ in (23) are needed for computing $\overline{\widehat{\mathcal{H}}}_j$ in (24).

4. APPLICATION EXAMPLES

In this section, we report numerical results we have obtained for two application examples of the polyreference subspace identification approach to structural vibration analysis proposed in section 3.4. The first one is a laboratory testbed, with which we investigate how sensors data in different directions and/or with different excitation directions can be merged. The second one is a real outdoor bridge, with which we investigate how to handle records with different numbers of moving sensors.

Before proceeding, some comments are in order on the practical use of the classical (monoreference and full covariance) subspace identification algorithm

of section 2.

4.1. SOME PRACTICAL ISSUES IN SUBSPACE EIGENSTRUCTURE IDENTIFICATION

The selection of the model order, and thus of the size of the Hankel matrices on one hand, and the handling of the presence and nature of excitation and measurement noises on the other hand, are two major practical issues which we address now.

As stressed in [5, 14, 12], when few sensors are available, a number of modes which is much smaller than the number of solutions of (2), but much larger than the number of sensors, can be identified. In order to extract the modes from the data, we have to apply the subspace method with an increasing SVD truncation order and to look for the relevant modes in the frequency band of interest. Since the subspace method yields a set of modes with both structural – from the structure *and* the excitation – and spurious mathematical modes, we have to derive a practical way to distinguish between the two types of modes. Fortunately, spurious modes tend to vary from one model order to the next. That is why usage suggests to plot the frequencies against SVD truncation order, in a stability or stabilization diagram [6, 12, 16]. This procedure is used in the sequel to display our results.

Numerous experiments with the classical subspace method have shown that :

- It is of no practical help to select for $\mathcal{H}_{p+1,q}$ in (5) other values than $q = p+1$. The number of lags $2p$ for the data covariances should be large (typically more than two hundreds in the experiments below).
- The number of modes should be overestimated, because modes tend to stabilize, and even to show up, for high orders. In other words, the SVD in the algorithm of section 2 should be truncated at an order much greater

than the 'theoretical' order, that is $2m/r - 1$, where m is the number of desired modes and r is the number of sensors.

An excitation noise at a single constant frequency is recognized as a pole by the algorithm of section 2, designed under the assumption of a white excitation noise. Such a pole can be eliminated provided that a prior information is available. This is the case of the harmonics of the rotation speed for rotating machines with load unbalancing. Similarly, a colored excitation noise can easily be eliminated provided that its poles are (significantly) more damped than those of the structure. It is also a common finding that the poles of the structure tend to stabilize when the Hankel matrix order is increased, whereas those of the excitation mostly do not. A nonstationary excitation is actually a favorable situation, since the averaging performed in (8) for computing G tend to whiten the noise. This is the case of a chirp-like nonstationary excitation.

Because of the above, the polyreference identification method has been implemented as follows. Since the Hankel matrix $\overline{\mathcal{H}}$ is built on stacked covariances (26), its SVD truncation order should be taken no greater than $q \times r_0/r$, where $r = r_0 + \sum_{j=1}^{J} r_j$, and where r_0 is the number of reference sensors and r_j the number of sensors in record j of (9).

4.2. LABORATORY EXAMPLE

We now show polyreference identification results obtained on the first application example, which is a laboratory setup.

4.2.1. *The steel-quake structure and its modes*

The steel-quake structure is used at the Joint Research Centre in Ispra (Italy) to test the performance of steel buildings during earthquakes. Exper-

Figure 1. The steel-quake structure.

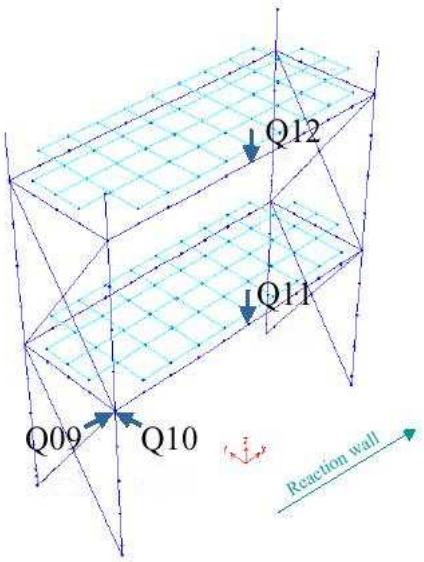

Figure 2. Steel-quake structure - Excitation impact locations: $Q09$ to $Q12$.

imental data from this structure have been proposed as a benchmark in the framework of the European COST F3 Structural Dynamics. The structure, shown in Figure 1, is a two-storey frame. The structure is excited with the aid of an impact hammer. The locations selected for the four impact tests are shown in Figure 2. For each impact location, eight to ten experiments are

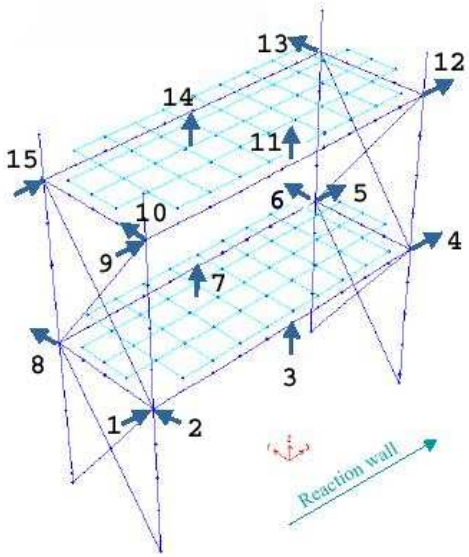

Figure 3. Steel-quake structure - Sensors locations, with directions summarized in Table 1.

Table 1

Steel-quake structure - Sensors directions, as displayed in Figure 3.

Sensor	1	2	3	4	5	6	7	8	9	10	11	12	13	14	15
Direct.	X	Y	Z	X	X	Y	Z	Y	X	Y	Z	X	Y	Z	X

performed, yielding data samples from the structure under different nonstationary excitations. Fifteen accelerometers are used for recording the reaction of the structure to the hammer impacts. The sampling frequency is 128 Hz, and for each channel 3200 data points are recorded. The sensor locations are shown in Figure 3, and the directions in which the measurements are taken are summarized in Table 1. Since the sensors locations are the same for the four impact tests, we can generate polyreference records as in (9) by selecting and grouping subsets of sensors from the different experiments. This results in nonstationary polyreference records corresponding to model (10,17).

The classical subspace algorithm of section 2, based on full data covariances

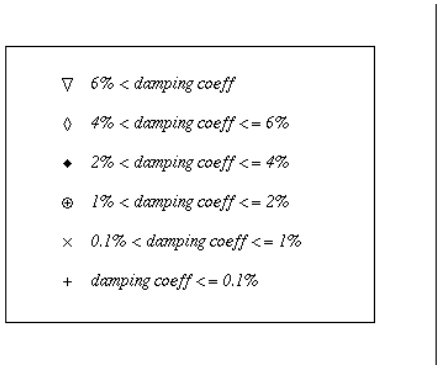

Figure 4. Meaning of the symbols used in Fig. 5 to 8, and Fig. 12 to 14.

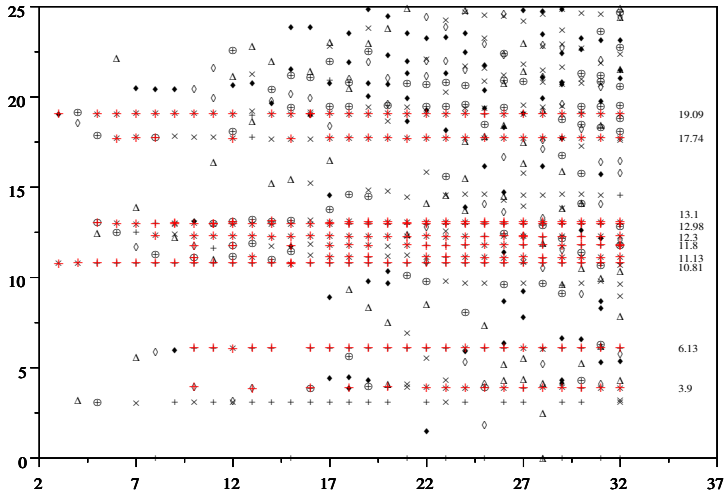

Figure 5. Steel-quake structure - Classical subspace identification - Twelve sensors (all except sensors 3, 7, 10) ($Q09-1$).

and on $q = 256$, has been applied to one set of twelve sensors data (all sensors except 3, 7, 10) from experiment $Q09-1$. The results are displayed in Fig. 5, where frequencies (ordinate) are displayed for increasing SVD truncation orders (abscissa), in a stabilization diagram which symbols are given in Fig. 4. Typical values and directions of the estimated modes which can be extracted are displayed in Table 2. This is in agreement with the results in [24].

Table 2

Steel-quake structure. Classical subspace identification - Some modes extracted from Fig. 5.

Mode	1	2	3	4	5	6	7	8
Freq.(Hz)	3.1	3.92	6.1	9.68	10.8	12.27	13.0	17.7
Direction	X	Y	Y	Y	X	Z	Z	Z

4.2.2. *Polyreference identification*

We have applied the polyreference algorithm of section 3.4 to different configurations, corresponding to different sensor locations, different hammer excitations, different excitation locations. In each of the figures 6 to 8, each record comes from a different excitation experiment. For example, in Fig. 6, the moving sensors we use are: sensors 11 and 14 from the first experiment of hammer location Q09, sensors 9 and 15 from the second experiment of hammer location Q10, sensors 1 and 4 from the third experiment of hammer location Q10, sensors 2 and 13 from the fourth experiment of hammer location Q09, and sensors 5 and 12 from the fifth experiment of hammer location Q10.

As mentioned in section 3.4, the computational cost of the method increases with the number of reference and moving sensors. However, the use of the low computational form of the SVD – which saves both memory space and computation time – makes it feasible to mix five records, each with four to five sensors. In that way, we have used almost all the sensors data available for the steel-quake benchmark.

The polyreference subspace identification algorithm, based on partial covariances (11) and on $q = 256$, has been applied to data from sessions $Q09$ to $Q12$, namely data merging the four excitations locations. However, since the results of all our experiments have not shown any qualitative difference

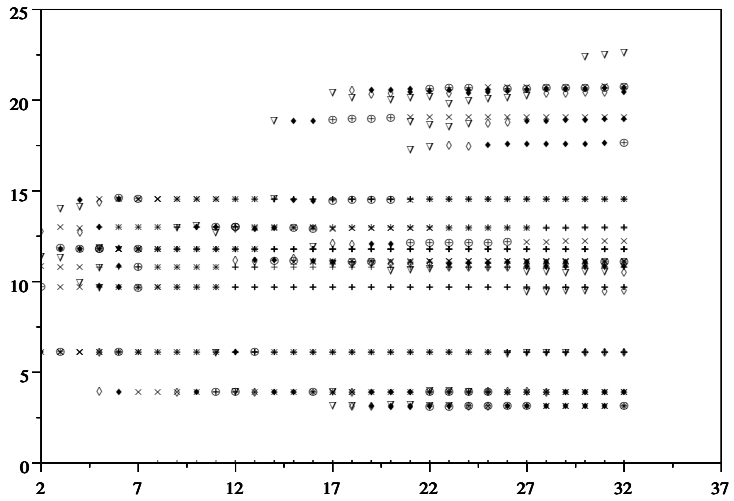

Figure 6. Polyreference: Ref. 6/8; Moving: 11/14 ($Q09-1$), 9/15 ($Q10-2$), 1/4 ($Q10-3$), 2/13 ($Q09-4$), 5/12 ($Q10-5$).

between using the four sessions and only the first two ones, in all the results shown below, the data which are used correspond to the excitation sessions $Q09$ and $Q10$ only.

Fig. 6 displays the stabilization diagram of a polyreference trial made with the sensors used for the results shown in Fig. 5. The two excitation cases are merged: data from experiments Q09 and Q10 are used. Even though the polyreference analysis handles covariance matrices of much smaller size (2×12) than the classical analysis (12×12), and is thus processing much less information, the stabilization diagram in Fig. 6 is obviously cleaned out from spurious modes which appear in the stabilization diagram of the classical algorithm in Fig. 5.

The stabilization diagram of a second polyreference trial merging experiments Q09 and Q10 is displayed on Fig. 7. Note that the diagram is good, even though the three reference sensors are in the three directions X, Y, and Z.

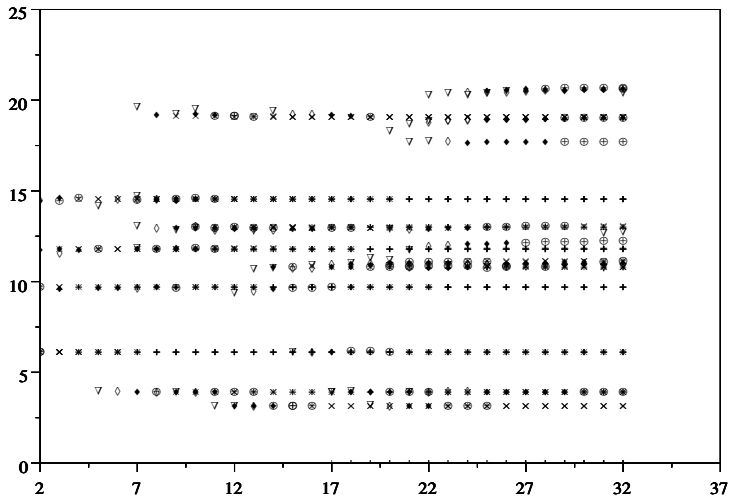

Figure 7. Polyreference: Ref. 1/6/7; Moving: 4/5 ($Q09-1$), 8/13 ($Q10-2$), 12/15 ($Q10-3$), 11/14 ($Q09-4$), 2/10 ($Q09-5$).

We now show a result suggesting how critical the grouping of the sensors in the pools of (10) is in influencing the extracted modeshapes. The stabilization diagram of a polyreference trial with all the sensors is displayed on Fig 8. Note that the sensors are grouped according to the direction in which they measure. Since all the available sensors are used, we plot the animated modeshapes [6] corresponding to three different frequencies: this is done in Fig. 9, Fig 10 and Fig 11. For each frequency, we have selected the modeshape with the highest MAC value. Taking the results in [24] as the reference modes and modeshapes, the modes and modeshapes in Fig. 8 to 11 are well identifed.

We point out that, theoretically, the eigenstructure identified by the polyreference method does not depend on the choice of the reference and moving sensors, but only on the whole set of sensors available. However, due to numerical

[6] In no measurement point all the DOF are measured; hence the animation lacks.

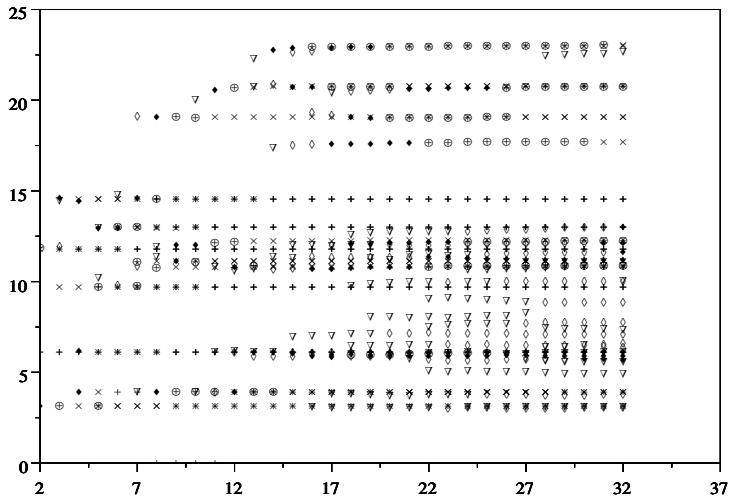

Figure 8. Polyreference: Ref.4/5/12; Moving: 1/9/15 ($Q10-1$), 2/6/8/10/13 ($Q10-2$), 3/7/11/14 ($Q10-3$).

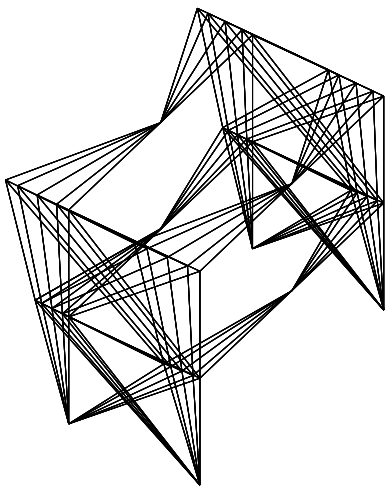

Figure 9. Modeshape extracted from Fig. 8 at 3.92 Hz.

precision, the polyreference method can be less stable than the classical subspace method. This can be seen sometimes on stabilization diagrams, which may not be the same for different choices of reference and moving sensors.

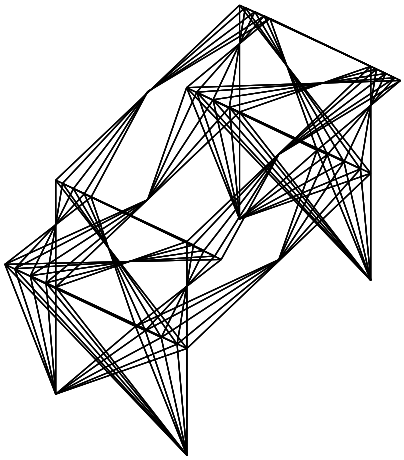

Figure 10. Modeshape extracted from Fig. 8 at 9.68 Hz.

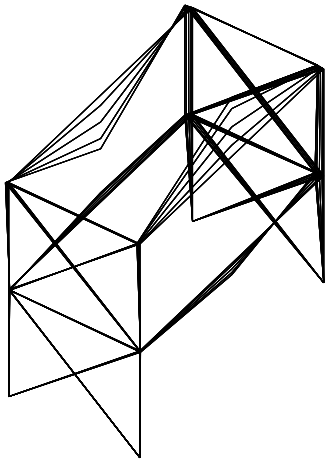

Figure 11. Modeshape extracted from Fig. 8 at 17.7 Hz.

But this effect may be more crucial for the modeshape extraction.

From numerous experiments, it turns out that a small number of sensors may be sufficient for finding many modes, provided that the sensors are well located, and in particular measure in the same direction. However, although

only few sensors are needed to extract frequencies and damping coefficients, processing more sensors is of interest to obtain modeshapes with a larger number of components, better suited for animation purposes.

4.3. REAL EXAMPLE

We now show polyreference identification results obtained on the second application example, which is a real bridge.

4.3.1. *The Z24 bridge and its modes*

The proposed method has been applied to the Swiss Z24 bridge, a benchmark of the BRITE/EURAM project SIMCES on identification and monitoring of civil engineering structures, for which EMPA[7] has carried out tests and data recording. The response of the bridge to traffic excitation under the bridge has been measured in 135 points, mainly in the vertical and transverse directions, and sampled at 100Hz. Because at most 19 sensors were available, 9 data sets have been recorded, each containing the measurements from 4 fixed and 15 moving sensors. However, it is not recommended to merge data recorded under too different temperature and traffic conditions [26], and to mix different directions [5]. Therefore, for investigating the experimental properties of the proposed polyreference subspace algorithm, we have selected $J = 2$ records from sensors in the vertical direction, with one reference sensor, and two moving sensors in the first record, and only one moving sensor in the second record. Each signal contains 65535 samples. As mentioned above, processing more records would have affected the required memory size, but *not* the computational complexity. Also, it is of interest to investigate the

[7] EMPA is the Swiss Federal Laboratories for Materials Testing and Research.

Table 3

Z24 bridge - Estimated modes - Classical subspace identification.

Mode	1	2	3	4	5
Freq.(Hz)	4.0	5.3	9.8	10.3	12.0

practical relevance of the conceptual capability of the proposed algorithm to handle records with different numbers of moving sensors.

The classical subspace algorithm of section 2, based on full data covariances and on $q = 128$, has been applied separately to each record, which contain 3 and 2 sensors, respectively. The results are displayed in Figure 12 and 13. Typical values of estimated modes which can be extracted from these diagrams are displayed in Table 3.

4.3.2. *Polyreference identification*

The polyreference subspace identification algorithm of section 3.4, based on partial covariances (11) and on $q = 128$, has been applied to the data from the two records. The results are displayed in Figure 14. Here, the SVD truncation order should be taken no greater than $128 \times 1/(1 + 2 + 1) = 32$. Figure 14 shows up several improvements over Figure 12 and Figure 13, on several aspects. Actually, for large enough truncation order:

- Spurious modes disappear: around 1 Hz, for example;
- True modes appear and stabilize faster and fluctuate less in the diagrams: around 5.3 Hz and 9.8 Hz, for example;
- The damping of the true modes is more accurately estimated, at lower orders than before, allowing to separate true and wrong modes among the stabilized ones: a wrong mode appears at 7 Hz with a high damping,

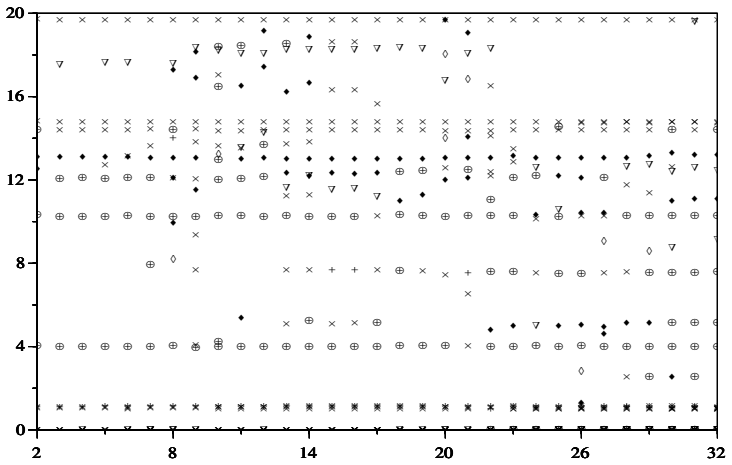

Figure 12. Z24 bridge - Classical subspace identification: first record (3 sensors).

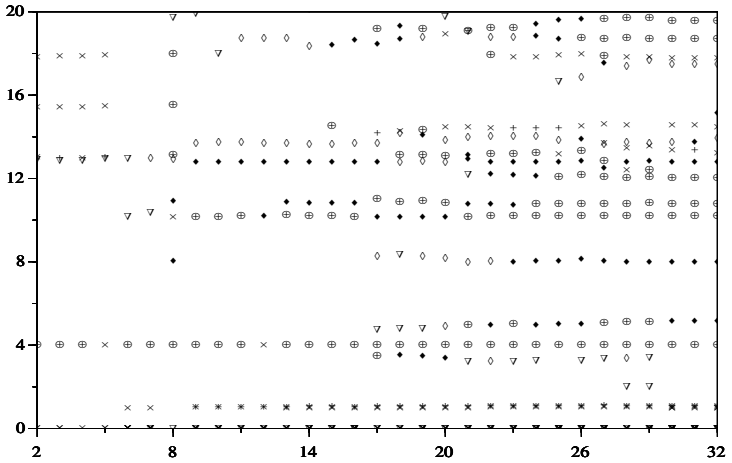

Figure 13. Z24 bridge - Classical subspace identification: second record (2 sensors).

whereas the true mode at 4 Hz appears with a low damping;

- Some modes, not identified on Figure 12 and 13, now show up in a stable diagram: around 12 Hz, among others.

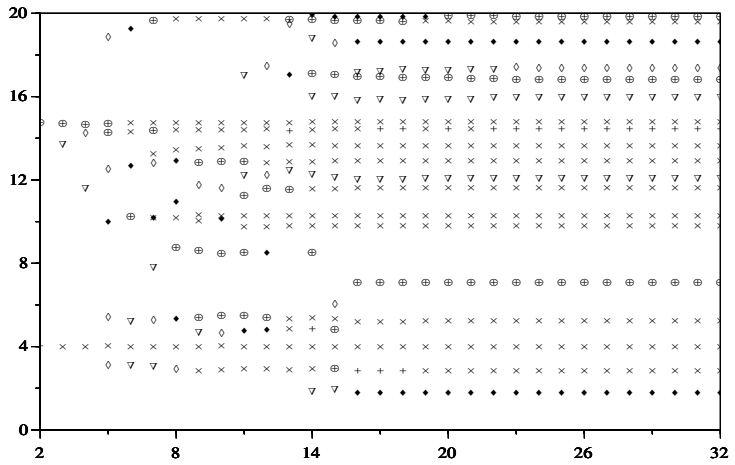

Figure 14. Z24 bridge - Polyreference subspace identification: merging the two records.

The polyreference method extracts seven modes in the range $0-11$ Hz. Five of these modes come from the structure and tend to appear in many diagrams during the whole year. The 5.3 Hz mode is very difficult to extract, due mainly to low excitation at this frequency. In both classical identifications (Figure 12 and 13), it appears very late in the diagrams and has little stability, whereas those two points are improved in the polyreference trial. Figure 14 is a remarkably clear diagram which, above a truncation order of 15, is cleaned from all spurious poles, even those which tend to stabilize in Figure 12 and 13. This appears to be an improvement w.r.t. the results in [16], where the stabilization diagrams resulting from merging different modal analyses are superimposed (but not smoothed) diagrams.

5. CONCLUSION

We have discussed the polyreference setup for output-only in-operation structural analysis. In this type of setup, several moving sensors mimic the availability of a much larger set of sensors. The proposed identification method consists in merging the data first and processing them globally using an output-only covariance-based subspace algorithm. This has to be contrasted with classical polyreference identification, which is usually performed by merging identification results obtained on the different records. The presence of an unmeasured and nonstationary excitation makes the issue of output data merging nontrivial. The key idea of the proposed method is a suitable normalization of the output covariances. This method, as well as the classical subspace identification algorithm [20], has been proved to provide us with consistent estimates of the eigenstructure, even under nonstationary excitation [23]. Numerical results on one laboratory setup (steelquake structure) and one real example (Z24 bridge) have been reported, which clearly highlight the potential benefits of the proposed method.

First, the method efficiently merges data by smoothing out the diagrams, rejecting spurious and instable frequencies. Actually, the averaging operation underlying the covariance computation, in combination with the key factorization property of the covariances, allows to cancel out nonstationarities in the excitation. Moreover, it appears that the introduction of different excitation conditions compensate somehow the loss of information due to the reduced size of the covariance matrices handled by the polyreference algorithm.

Second, even with short record lengths, the natural frequencies are well estimated, whereas the modeshapes are more sensitive to the record length;

this is in agreement with the results obtained for a bridge reported in [25].

Third, applying the polyreference method over time is expected to smooth out further the effect of nonstationary excitation. Finally, the actual stability of the polyreference diagrams makes the proposed polyreference method a good candidate for a future automated identification procedure.

What the proposed algorithm is not capable of is to separate modes of the structure from the modes corresponding to the non–white excitation, but the classical subspace identification procedure is unable to achieve that either. Nevertheless, the new algorithm appears to perform well at extracting modes which appear only in some diagrams, for example modes which are not very well excited all the time. This feature is important in practice, and should hopefully be confirmed in further numerical investigations.

Acknowledgement

Part of this work has been carried out within the framework of Eureka project 1562 SINOPSYS (model based **S**tructural monitoring using **IN-OP**eration **SYS**tem identification), coordinated by LMS, Leuven, Belgium.

References

1. L. Hermans and H. Van der Auweraer 1999 *Mechanical Systems and Signal Processing*, **13**, 193–216. Modal testing and analysis of structures under operational conditions: industrial applications.
2. E. Parloo, P. Verboven, P. Guillaume and M. Van Overmeire 2001 *Proceedings of the International Modal Analysis Conference*, 425–431. Maximum likelihood identification of modal parameters from nonstationary operational data.
3. D.J. Ewins 1984 *Modal Testing: Theory and Practice*, Research Studies Press, Letchworth, Hertfordshire, UK.
4. J.N. Juang 1994 *Applied System Identification*, Prentice Hall, Englewood Cliffs, NJ.

5. M. Prevosto, M. Olagnon, A. Benveniste, M. Basseville and G. Le Vey 1991 *Jal Sound and Vibration*, **148**, 329–342. State-space formulation, a solution to modal parameter estimation.
6. R.J. Allemang and D.L. Brown 1998 *Journal of Sound and Vibration* **211**, 301–322. A unified matrix polynomial approach to modal identification.
7. Q.J. Yang, P.Q. Zhang, C.Q. Li and X.P. Wu 1994 *Mechanical Systems and Signal Processing*, **8**, 159–174. A system theory approach to multi-input multi-output modal parameters identification methods.
8. F. Deblauwe, R.J. Allemang and D.L. Brown 1987 *Proceedings of the International Modal Analysis Conference*, 832–845. The polyreference time domain technique.
9. B. Ottersten, M. Viberg and T. Kailath 1992 *IEEE Trans. Signal Processing*, **40**, 590–599. Analysis of subspace fitting and ML techniques for parameter estimation.
10. P. Van Overschee and B. De Moor 1996 *Subspace Identification for Linear Systems: Theory, Implementation, Applications*, Kluwer.
11. M. Viberg and B. Ottersten 1991 *IEEE Trans. Signal Processing*, **39**, 1110–1121. Sensor array processing based on subspace fitting.
12. B. Peeters and G. de Roeck 1999 *Mechanical Systems and Signal Processing*, **13**, 855–878. Reference-based stochastic subspace identification for output-only modal analysis.
13. G. de Roeck, B. Peeters and W.-X. Ren 2000 *Proceedings of the International Modal Analysis Conference*, 1106–1112. Benchmark study on system identification through ambient vibration measurements.
14. M. Basseville, A. Benveniste, B. Gach-Devauchelle, M. Goursat, D. Bonnecase, P. Dorey, M. Prevosto and M. Olagnon 1993 *Mechanical Systems and Signal Processing*, **7**, 401–423. Damage monitoring in vibration mechanics: issues in diagnostics and predictive maintenance.
15. M. Abdelghani, M. Goursat, T. Biolchini, L. Hermans and H. Van der Auweraer 1999 *Proceedings of the International Modal Analysis Conference*, 224–230. Performance of output-only identification algorithms for modal analysis of aircraft structures.
16. H. Van der Auweraer, W. Leurs, P. Mas and L. Hermans 2000 *Proceedings of the International Modal Analysis Conference*, 763–771. Modal parameter estimation from inconsistent data sets.
17. R.L. Mayes and S.E. Klenke 2001 *Proceedings of the International Modal Analysis Conference*, 1023–1028. Consolidation of modal parameters from several extraction sets.
18. P. Stoïca and R.L. Moses 1997 *Introduction to Spectral Analysis*, Prentice Hall.
19. H. Akaïke 1974 *IEEE Trans. on Automatic Control*, **19**, 667–674. Stochastic theory of minimal realization.
20. A. Benveniste and J-J. Fuchs 1985 *IEEE Trans. Automatic Control* **30**, 66–74. Single sample modal identification of a nonstationary stochastic process.

21. H. Akaïke 1973 *SIAM Jal Control*, **13**, 162–173. Markovian representation of stochastic processes by canonical variables.
22. M. Basseville, M. Abdelghani and A. Benveniste 2000 *Automatica* **36**, 101–109. Subspace-based fault detection algorithms for vibration monitoring.
23. L. Mevel, A. Benveniste, M. Basseville and M. Goursat 2000 *IRISA Research Report* **1354**. Blind subspace-based eigenstructure identification under nonstationary excitation using moving sensors.
24. J.B. Bodeux and J.C. Golinval 2000 *Proceedings of the European COST F3 Conference on System Identification and Structural Health Monitoring*, 303–312. ARMAV model technique for system identification and damage detection.
25. C. Gentile and A. Saisi 2000 *Proceedings of the International Modal Analysis Conference*, 1320–1326. Accuracy assessment of bridge modal parameters estimated from ambient vibration measurements.
26. B. Peeters and G. de Roeck 2000 *Proceedings of the International Modal Analysis Conference*, 1570–1576. One year monitoring of the Z24-bridge: environmental effects versus damage events.